Chemical Engineering Journal 204–206 (2012) 1–7

Contents lists available at SciVerse ScienceDirect

Chemical Engineering Journal

journal homepage: www.elsevier.com/locate/cej

PbS-sensitized $K_2Ti_4O_9$ composite: Preparation and photocatalytic properties for hydrogen evolution under visible light irradiation

Wenquan Cui *, Shanshan Ma, Li Liu, Yinghua Liang *

College of Chemical Engineering, Hebei United University, Tangshan 063009, PR China

HIGHLIGHTS

- PbS was deposited on the surface of $K_2Ti_4O_9$ via a precipitate method.
- The deposition of PbS greatly increase the visible light absorption for $K_2Ti_4O_9$.
- The composite photo-catalysts exhibited enhanced photocatalytic hydrogen evolution.

GRAPHICAL ABSTRACT

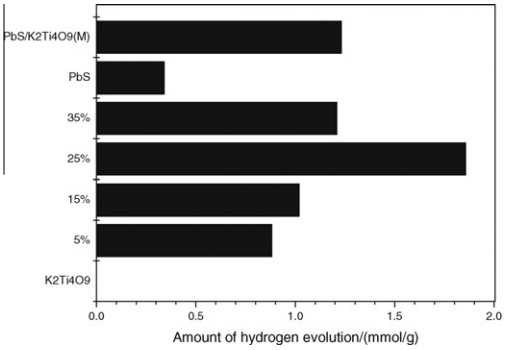

ARTICLE INFO

Article history:
Received 23 April 2012
Received in revised form 16 July 2012
Accepted 17 July 2012
Available online 25 July 2012

Keywords:
PbS
$K_2Ti_4O_9$
Deposition–precipitation
Photo-catalysis
Hydrogen evolution

ABSTRACT

PbS-sensitized $K_2Ti_4O_9$ composite photo-catalysts (hereafter designated as PbS/$K_2Ti_4O_9$) were prepared by a facile deposition–precipitation method. The samples were characterized by scanning electron microscopy (SEM), energy dispersive X-ray (EDS), X-ray diffraction (XRD), ultraviolet–visible diffuse reflectance spectra (UV–Vis DRS), X-ray photoelectron spectroscopy (XPS) and photoluminescence measurement (PL). The photo-catalytic activities were investigated under visible light irradiation. The results indicated that the size of PbS, which uniformly scattered on the surface of $K_2Ti_4O_9$, distribute in the range of 50–100 nm. The absorption edge of $K_2Ti_4O_9$ shifted to the visible light region and recombination of electrons and holes was suppressed after the deposition of PbS. The composite photo-catalyst loading 25 wt.% PbS synthesized by deposition–precipitation method showed the highest photo-catalytic activity. The amount of hydrogen evolution is 1.85 mmol/g after 3 h irradiation over 0.5 g catalyst in the reaction system containing Na_2S–Na_2SO_3–KOH aqueous solution. Finally, the mechanism of the photo-catalysis was discussed.

1. Introduction

In recent years, layered compound semiconductors have been aroused increasing attention as new type photo-catalysts. Layered compound catalyst whose structure is similar to mica or clay is a kind of layered semiconductor metal oxide. Compared to bulk photo-catalyst, the outstanding advantage of layered semiconductor oxide is the two-dimensional interlayer structure act as photo-catalytic water splitting reaction site, thus the photo-induced electrons can transfer to the surface of catalyst efficiently, while the photo-induced holes stay in the layered space [1–3]. Thereby the recombination of electron–hole pair would be suppressed effectively, and improve the photocatalytic reaction performance. Layered compound catalysts are considered to be a series of potential photo-catalysts and have become one of the hotspots in the field of photo-catalysis [4–7].

$K_2Ti_4O_9$ is a two-dimensional layered compound, which is formed by the connection of octahedral units of TiO_6 and oxygen bridging atoms [8]. Previous report [9] shows that $K_2Ti_4O_9$

* Corresponding authors. Tel.: +86 13292508307 (W. Cui), tel.: +86 315 2592014 (Y. Liang).
E-mail addresses: wkcui@163.com (W. Cui), liangyh@heuu.edu.cn (Y. Liang).

1385-8947/$ - see front matter © 2012 Elsevier B.V. All rights reserved.
http://dx.doi.org/10.1016/j.cej.2012.07.075

exhibited high activity for hydrogen evolution from methanol solution under UV light irradiation. However, the band gap of $K_2Ti_4O_9$ is ca. 3.2–3.4 eV [10], which cannot be excited under visible light, that is $K_2Ti_4O_9$ can hardly exhibit photocatalytic activity under visible light irradiation. One of the common way to increase the visible light response for $K_2Ti_4O_9$ is to introduce narrow band-gap semiconductors, such as Fe_2O_3 [11], CdS [12,13], into the layered space. In our previous study [14], we have synthesized PbS intercalated $K_2La_2Ti_3O_{10}$ photocatalyst, where PbS located in the layered space of $K_2La_2Ti_3O_{10}$, which revealed that PbS can greatly increase the photocatalytic capacity under visible light irradiation. The narrow band-gap semiconductor not only acts as the sensitizer, but also reduces the recombination rate of the photo-generated electron–hole pair and gives rise to an enhancement of the photo-catalytic activity [15–17]. However, one of the main drawbacks is a complicated synthesis procedure, which includes acid exchange, amine pillared and iron exchange and often takes at least 1 week, hindering the practical application of intercalated $K_2Ti_4O_9$ significantly. Furthermore, it is hard to control the precise amount of intercalated semiconductor, and the structure of the layered compound may be changed dramatically after intercalation [18]. The intercalation reaction for titanate-layered compounds is also more difficult to achieve, due to their high charge density [19,20]. Consequently, it is of great importance to adopt a simple and fast synthesis procedure on the basis of not changing the crystal form of layered compound to enhance the photo-catalytic activity in the visible region.

In view of above description, we synthesized surface PbS-modified $K_2Ti_4O_9$ composite photo-catalyst by depositing the narrow band-gap PbS particles on the surface of $K_2Ti_4O_9$ via a facile deposition–precipitation method. Utilizing the sensitization effect of PbS to improve $K_2Ti_4O_9$ visible light responsible range and promoting separation of photo-induced carriers, are of great importance to further improve photo-catalysis activity of layered compound catalysts. Until now, to our knowledge, such research has not been reported. Meanwhile, the as-prepared composites were characterized by SEM, EDS, XRD, UV–Vis DRS, XPS, PL and investigated the photo-catalytic activity of hydrogen evolution from water under visible light irradiation. Finally, reaction mechanism was analyzed in the present work.

2. Experimental

2.1. Synthesis of photocatalysts

All chemicals were reagent grade and used without further purification. $K_2Ti_4O_9$ powders were prepared by a solid-phase reaction. The detailed procedure is as follows: a mixture of TiO_2 and anhydrous K_2CO_3 (molar ratio 4:1.1) was ground sufficiently in agate mortar with a defined amount of absolute ethyl alcohol. Then the ground mixture was calcinated in muffle at 1000 °C for 12 h.

The PbS/$K_2Ti_4O_9$ sample was prepared via a deposition–precipitation method. $K_2Ti_4O_9$ powder and $SC(NH_2)_2$ aqueous solution were dissolved into ammonia (14.4 M) and then a certain amount of $Pb(CH_3COO)_2$ aqueous solution was slowly added drop-wise to the above mixtures under continuous stirring. After that, the mixed suspensions were refluxed for 1 h. The resulting suspension was filtered, and then washed with deionized water and ethanol, respectively. The material was dried at 110 °C for 3 h. The process could be described by the following reaction:

$$Pb(NH_3)_n^{2+} + SC(NH_2)_2 + 2OH^- \rightarrow PbS + 2H_2O + CN_2H_2 + 2nNH_3$$

In order to compare, the additional samples were synthesized: (1) PbS/$K_2Ti_4O_9$(M) photo-catalyst, which was synthesized via the simple mechanical mixing of a certain proportion of PbS and $K_2Ti_4O_9$ powders. (2) TiO_2, which was synthesized by a precipitation method. A certain concentration of ammonia was mixed drop-wise with $Ti(SO_4)_2$ aqueous solution and the mixture was continuously stirred at room temperature for 1 h. The precipitated powder was filtered, and washed with deionized water and ethanol respectively, then dried at 80 °C for 3 h. Finally, the dried power was calcined at 600 °C for 2 h. (3) PbS/TiO_2, whose synthesize method was similar with that of PbS/$K_2Ti_4O_9$. (4) Pure PbS, which was synthesized by a precipitation method with $Pb(CH_3COO)_2$, $SC(NH_2)_2$ and ammonia.

2.2. Characterization of the photocatalysts

The crystal structure and the phase of the samples were determined by X-ray diffractometer (XRD) using a Rigaku D/MAX2500 PC diffractometer with Cu Kα radiation, with an operating voltage of 40 kV and an operating current of 100 mA. The morphology of the samples was detected using a scanning electron microscope (SEM) (Hitachi, s-4800). UV–vis light (UV–vis) diffuse reflectance spectra were recorded on a UV–vis spectrometer (Puxi, UV1901). The chemical compositions of the sample were tested by an energy dispersive X-ray detector (EDX, Thermo Noran 7). The chemical states of the photo-catalysts were analyzed by XSAM800 X-ray photoelectron spectroscopy (XPS). The luminescence (PL) of the powdered samples was measured on a spectrofluorometer (Hitachi, f7000).

2.3. Photo-catalytic activity

The photocatalytic activities of hydrogen production for the photocatalyst samples were examined in an inner irradiation system. Typically, 0.5 g powder of photo-catalyst was dispersed in a Pyrex reaction cell containing 250 ml of aqueous solution of 0.1 M Na_2S, 0.5 M Na_2SO_3 and 1 M KOH. Thermostatic water flowed through a jacket between the light source and the reaction cell to remove extra heat produced by the lamp. The light source used was a 500 W xenon lamp (the light with $\lambda < 400$ nm was filtered out by flowing 1 M $NaNO_2$ solution in the jacket between the xenon lamp and the reaction cell). The suspensions were deairated with Ar gas for 30 min to prevent uptake of photo-generated electrons by dissolved oxygen before irradiation. The produced hydrogen gas was detected using an online gas chromatography system (FULI-GC9790, molecular sieve 5 A column, TCD detector, Ar carrier). Ar gas was used as a carrier for the products.

3. Results and discussion

3.1. Characterization of catalysts

The morphologies of $K_2Ti_4O_9$, PbS/$K_2Ti_4O_9$, PbS/$K_2Ti_4O_9$(M) and pure PbS photocatalysts were observed using SEM. Fig. 1a presents a typical SEM image of the pure $K_2Ti_4O_9$, which showed needle-like shape particles with the stacks of layered structure. From Fig. 1a, it can be seen that the $K_2Ti_4O_9$ particles exhibits nonuniform size distribution, varying from 1–4 μm long and 0.5–2 μm wide. Fig. 1b is the image of PbS deposited on $K_2Ti_4O_9$. The PbS nanoparticles are uniformly distributed on the surface of $K_2Ti_4O_9$, and no obvious change is observed in the morphology of $K_2Ti_4O_9$ after being composed with PbS, which indicating that the deposition process did not damage the $K_2Ti_4O_9$ structure. The PbS particles, which are scattered on the surface of $K_2Ti_4O_9$, have a relatively uniform size distribution of approximately 50–100 nm and show relatively good dispersity. Fig. 1c shows the SEM image of mechanical mixing with PbS and $K_2Ti_4O_9$. It can be observed that mechanical mixing process did not change the surface morphology of $K_2Ti_4O_9$ either,

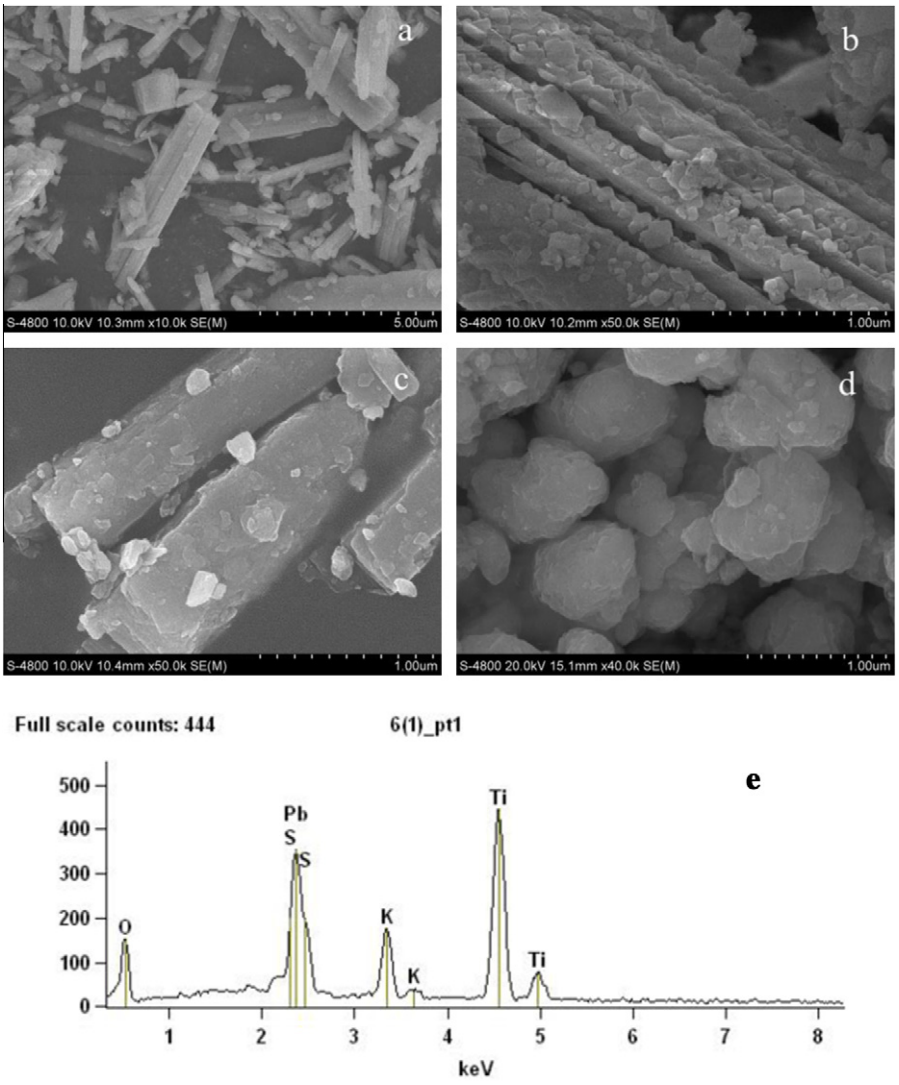

Fig. 1. SEM images of photo-catalyst: (a) $K_2Ti_4O_9$, (b) PbS(25 wt.%)/$K_2Ti_4O_9$, (c) PbS(25 wt.%)/$K_2Ti_4O_9$(M), (d) PbS and (e) corresponding EDS pattern of (b).

but PbS particles distribute nonuniformly and the size of them is larger. In Fig. 1d, the morphology of PbS is irregular spherical particles of about 500 nm. The image demonstrates the presence of agglomerated particles, whose size is much bigger than that of PbS/$K_2Ti_4O_9$, indicating that the precipitation method resulted in large and nonuniform particles of pure PbS. Fig. 1e shows the typical EDX spectrum obtained from PbS(25 wt.%)/$K_2Ti_4O_9$. In the spectrum, peaks associated with O, S, Pb, K, and Ti were observed. K, Ti, and O peaks result from $K_2Ti_4O_9$, and Pb and S result from PbS, respectively. The spectrum confirms the corresponding chemical elements for composite catalyst and no other elements were detected.

Fig. 2 shows the XRD patterns of PbS, $K_2Ti_4O_9$ and PbS/$K_2Ti_4O_9$, respectively. The characteristic diffraction peaks for PbS at 2θ of 25.968°, 30.074°, 43.050°, 50.965°, 53.406°, 62.515° and 68.865° were attributed to the (111), (200), (220), (311), (222), (400) and (331) crystal planes of PbS crystal, which was indexed to PbS (JCPDS 65-0346). PbS crystallized in a face centered cubic system (rock salt NaCl structure, the cell parameter a = 593.8 nm). The diffraction peaks were relatively acute and no evident impurity peaks were observed which revealed that the as-prepared catalyst had a higher crystallinity. The diffraction peaks for $K_2Ti_4O_9$ and PbS/$K_2Ti_4O_9$ appearing at 2θ of 10.089°, 14.297°, 31.026° and

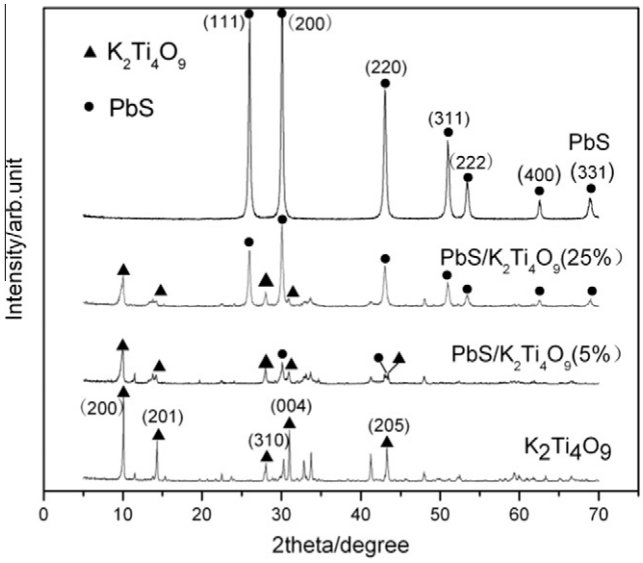

Fig. 2. XRD patterns of PbS, $K_2Ti_4O_9$ and PbS/$K_2Ti_4O_9$.

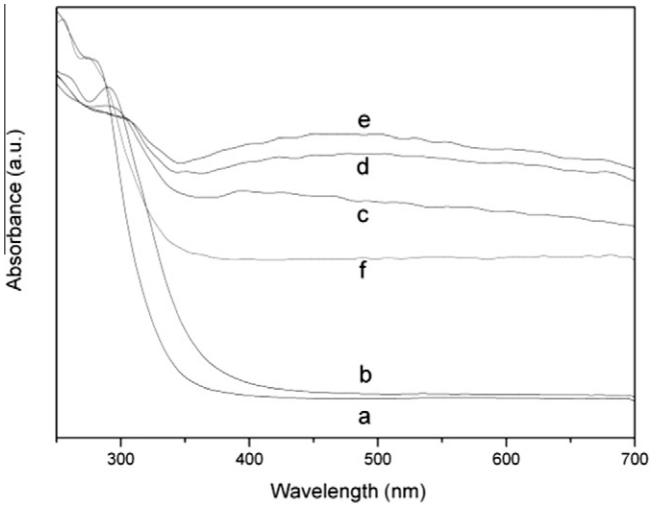

Fig. 3. UV–vis diffuse reflectance spectra of photo-catalysts: (a) $K_2Ti_4O_9$, (b)PbS (5 wt.%)/$K_2Ti_4O_9$, (c) PbS(15 wt.%)/$K_2Ti_4O_9$, (d) PbS(25 wt.%)/$K_2Ti_4O_9$, (e) PbS(35 wt.%)/$K_2Ti_4O_9$ and (f) PbS(25 wt.%)/$K_2Ti_4O_9$(M).

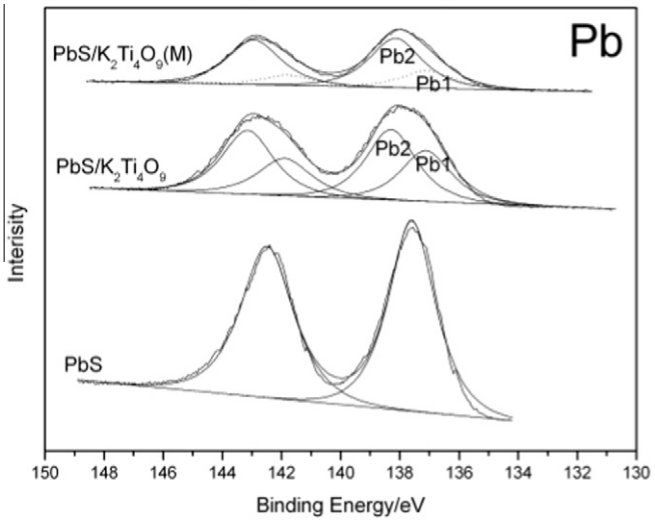

Fig. 4. Pb XPS spectrum of different sample.

43.275° were assigned to (200), (201), (004) and (205) crystal planes of monoclinic $K_2Ti_4O_9$ (JCPDS 32-0861). These facts indicated that the layered perovskite structure of $K_2Ti_4O_9$ did not change after deposition of PbS. When the amount of PbS was 5 wt.% in PbS/$K_2Ti_4O_9$, major XRD patterns for composite catalyst were still attributed to $K_2Ti_4O_9$. Other small peaks could be assigned to PbS (200), (220) crystal planes due to the low proportion of PbS. The apparent diffraction peaks for PbS were observed in PbS(25 wt.%)/$K_2Ti_4O_9$ photocatalyst, yet the peaks corresponding to $K_2Ti_4O_9$ weakend evidently. We could conclude that the surface of $K_2Ti_4O_9$ was covered by PbS particles.

Fig. 3 shows the UV–vis diffuse reflectance spectra of photo-catalysts. The absorption edge of $K_2Ti_4O_9$ was observed at approximately 350 nm, corresponding to a band gap of 3.54 eV. Therefore, it could only absorb UV rather than visible light. $K_2Ti_4O_9$, sensitized by PbS, showed visible light absorption ability, not only absorbed the light below the wavelength of 350 nm. It is owing to the band gap of PbS being 0.41 eV [21], so PbS could absorb a majority of visible light. It could also be found that the absorption intensity of the composite catalysts changed with altering of PbS amount (5–35 wt.%). When the loading amount of PbS was 5 wt.%, the absorption curve of PbS/$K_2Ti_4O_9$ was close to that of $K_2Ti_4O_9$, which indicated that a small amount of the external surface of $K_2Ti_4O_9$ was covered by PbS. The absorption intensity in the visible light region of the composite catalysts increased with an increase of PbS, indicating that the external surface of $K_2Ti_4O_9$ was gradually covered with the increase of PbS. When the amount of PbS reached 35 wt.%, the absorption inflection of $K_2Ti_4O_9$ was less noticeable, indicating most of the surface of $K_2Ti_4O_9$ was covered by PbS. Furthermore, the absorbance intensity of the PbS(25 wt.%)/$K_2Ti_4O_9$(M) synthesized by direct mechanical mixing was between the absorbance intensity of the PbS(5 wt.%)/$K_2Ti_4O_9$ and PbS(15 wt.%)/$K_2Ti_4O_9$, but lower than that of PbS(25 wt.%)/$K_2Ti_4O_9$. This may suggest that the precipitation procedure resulted in a uniform PbS distribution on the surface of $K_2Ti_4O_9$ and made the particle size of PbS smaller.

The X-ray photoelectron spectroscopy (XPS) analysis was carried out in order to determine the chemical composition of the synthesized samples and the valence states of surface elements. Figs. 4–7 show the XPS spectra of Pb 4f (Fig. 4), S 2p (Fig. 5), Ti 2p (Fig. 6), and O 1s (Fig. 7) for different samples respectively. As shown in Fig. 4, the binding energy of Pb 4f5/2 and Pb 4f7/2 for pure PbS appeared at 142.5 and 137.6 eV respectively and the spin orbit splitting energy was found to be 4.9 eV. In PbS/$K_2Ti_4O_9$, the Pb

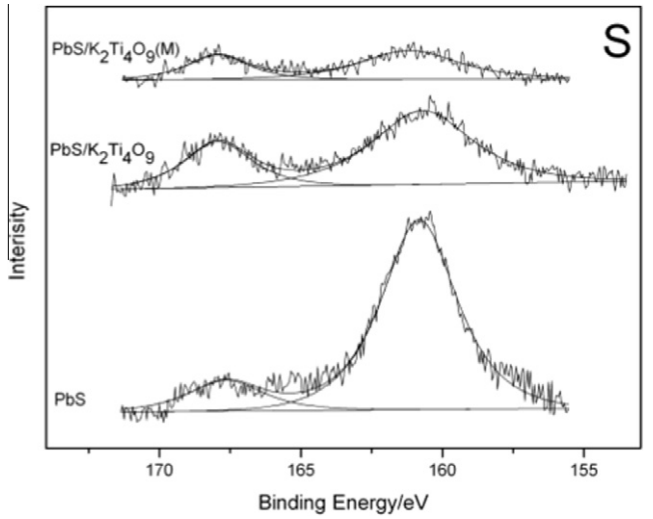

Fig. 5. S XPS spectrum of different sample.

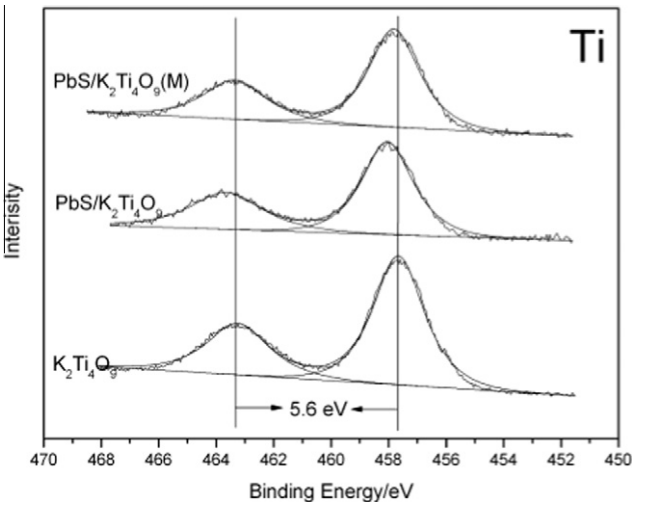

Fig. 6. Ti XPS spectrum of different sample.

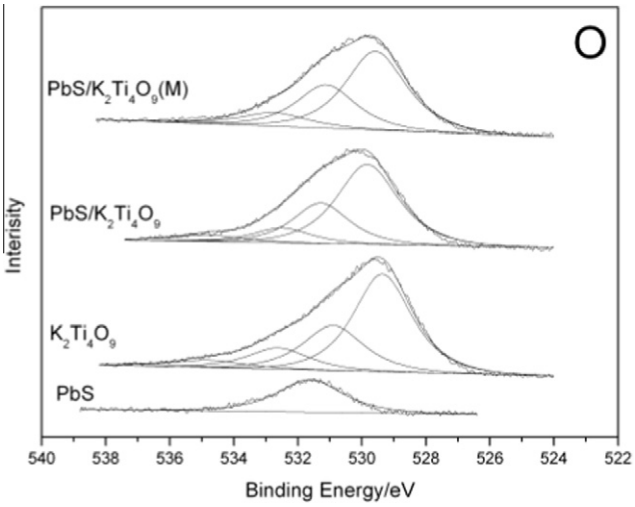

Fig. 7. O XPS spectrum of different sample.

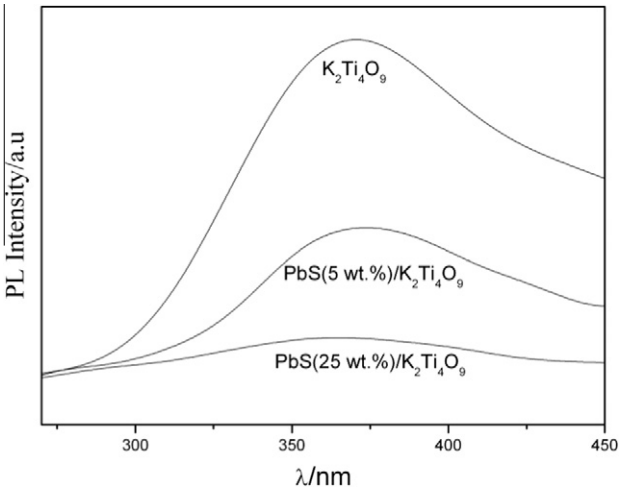

Fig. 8. The fluorescence spectra of catalysts (λ_{ex} = 230 nm).

4f7/2 peak was resolved into two bands, P1 and P2, by fitting it into Voigt function. The P1 band at 137.0 eV and the P2 band at 138.3 eV were assigned to the Pb–S and Pb–O bonding structures, respectively. The Pb–O band had a much lower intensity in the $PbS/K_2Ti_4O_9$(M) [22]. The binding energy of Pb for $PbS/K_2Ti_4O_9$ was lower than that of pure PbS, which may indicate a higher electronic density of Pb^{2+} in $PbS/K_2Ti_4O_9$ than that in pure PbS. The XPS spectrum of S 2p is shown in Fig. 5. The S 2p orbit showed two peaks at 160.8 eV and 167.6 eV, which were assigned to S^{2-} and S^{6+} [23], respectively. The existence of S^{6+} indicated that the surface of PbS was exposed to air after synthesis process [24]. As shown in Fig. 6, the Ti 2p peaks for pure $K_2Ti_4O_9$ were well deconvoluted by two curves at approximately 463.2 and 457.6 eV, which could be attributed to spin orbit components of 2p1/2 and 2p3/2, respectively. A spin orbit splitting energy between Ti 2p1/2 and Ti 2p3/2 was found to be 5.6 eV, which corresponds to Ti^{4+} [23]. The peaks of Ti 2p for $PbS/K_2Ti_4O_9$ were centered at 463.7 and 458.0 eV. The binding energy of Ti 2p increased by up to 0.5 and 0.4 eV compared to that of pure $K_2Ti_4O_9$, respectively, demonstrating that the surrounding electronic density of Ti decreased after loading PbS on $K_2Ti_4O_9$ via the precipitation method. The binding energy of Pb and Ti changed. We deduced that Ti–O–Pb may exist in $PbS/K_2Ti_4O_9$ composite, due to the fact that the electronegativity of Pb is 2.33, which is larger than that of Ti (1.54) according to Pauling Scale [25]. Pb^{2+} with higher electronegativity decrease the surrounding electronic density of Ti, resulting in screening effect reduced, so binding energy of Ti2p increased. While in $PbS/K_2Ti_4O_9$(M) synthesized by mechanical mixing, the binding energy changed less, which indicated that the contact between two phases of catalyst synthesized by mechanical mixing not closely enough and the ion spread phenomenon was not obvious. The XPS peaks of O 1s for the samples are shown in Fig. 7. The peak centered at the binding energy of 531.6 eV was assigned to hydroxyl oxygen, which may indicate that hydroxyl groups are induced during the preparation of PbS. The O1s peaks for $K_2Ti_4O_9$, with binding energies located at 532.6, 530.9 and 529.4 eV, were assigned to the adsorbed oxygen, hydroxyl oxygen and lattice oxygen, respectively. The exist of adsorbed oxygen demonstrate adsorbed oxygen gas molecules deposit on the surface of $K_2Ti_4O_9$; The exist of hydroxyl oxygen demonstrate that there are trace of water molecules on the surface of $K_2Ti_4O_9$; The peak of lattice oxygen demonstrates the exist of Ti–O–Ti structure. Adsorbed oxygen included chemical and physical state, and binding energy decrease of which indicated that it changed from physical adsorption to chemical adsorption.

Molecular fluorescence spectroscopy is a kind of emission spectrum caused by the electron–hole recombination, which can reflect the migration and capture of photo-induced carriers [26]. The results obtained for the prepared samples are shown in Fig. 8. As can be seen from the PL spectra, in the range of 270–450 nm, photo-luminescence intensities decreased in the order of $K_2Ti_4O_9$ > $PbS(5\ wt.\%)/K_2Ti_4O_9$ > $PbS(25\ wt.\%)/K_2Ti_4O_9$. The emission peak at 370 nm in $K_2Ti_4O_9$ could be related to a recombination of the conduction band electron with valence band hole within the semiconductor. The peak remained at the same position upon combination of $K_2Ti_4O_9$ with PbS, but the intensity decreased, indicating that energy bands coupled in $PbS/K_2Ti_4O_9$ composite catalyst. The photo-induced holes in the VB of $K_2Ti_4O_9$ irradiated by UV-light could be transferred to the VB of PbS, leading to the decrease of holes in the VB of $K_2Ti_4O_9$. After electrons in the CB of $K_2Ti_4O_9$ moved back to the VB, the recombination probability of them with holes decreased, resulting in a weaken emission peak intensity. In addition, the PL intensity of $PbS(25\ wt.\%)/K_2Ti_4O_9$ was lower than that of $PbS(5\ wt.\%)/K_2Ti_4O_9$, indicating that higher PbS loading amount was favorable for the recombination of photogenerated charge carriers.

3.2. Photocatalytic activities for hydrogen production over photo-catalysts

Fig. 9 shows the comparison of hydrogen production activity of $PbS/K_2Ti_4O_9$ and PbS/TiO_2 under visible light irradiation. It can be clearly observed that the activity of $PbS/K_2Ti_4O_9$ is much higher than that of PbS/TiO_2. The valence and conduction band for $K_2Ti_4O_9$ are +3.0 eV and −0.54 eV [27], respectively, while the valence and conduction band of TiO_2 are 3.01 and −0.19 eV vs NHE [28], respectively. The position of conduction band edge of $K_2Ti_4O_9$ is higher than that of TiO_2, which indicates that the potential of $K_2Ti_4O_9$ is more negative than the redox potential of H^+/H_2, leading to a greater redox capacity. Besides, in comparison with the bulk TiO_2 catalyst, $K_2Ti_4O_9$ is an n-type semiconductor with a layered two-dimensional structure space [8], where the photo-induced electrons or holes could be restricted, so that the recombination of electrons and holes can be reduced [29]. Therefore, the electrons, which are generated from the conduction band of PbS, can be transferred to the conduction band of $K_2Ti_4O_9$, and then further migrate into the layered space of $K_2Ti_4O_9$ [9], while the holes will still stay in the valence band of PbS. This process promoted the separation of photo-induced hole–electron pairs.

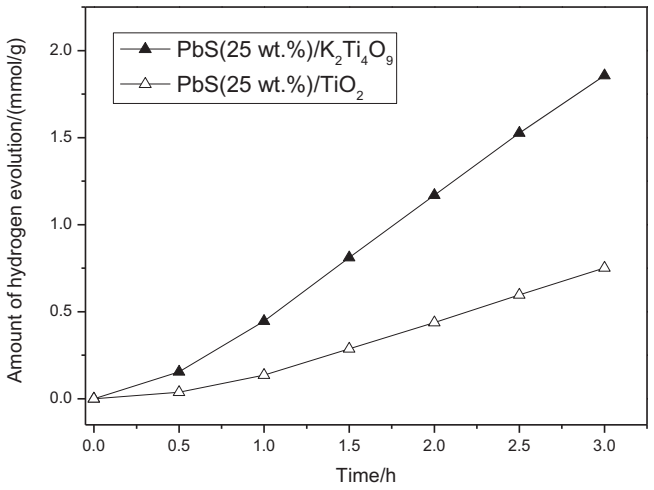

Fig. 9. Hydrogen evolution over $PbS/K_2Ti_4O_9$ and PbS/TiO_2 under visible light.

In the present work, the photo-catalytic performances of $PbS/K_2Ti_4O_9$ catalysts were investigated by measuring photo-catalytic hydrogen evolution under visible light irradiation for 3 h. The activities of hydrogen evolution over $PbS/K_2Ti_4O_9$(M), $PbS/K_2Ti_4O_9$, $K_2Ti_4O_9$ and PbS observed are shown in Fig. 10. As seen from Fig. 10, no H_2 was detected on pure $K_2Ti_4O_9$ photo-catalyst under visible light, which may be associated with the fact that it absorbs UV-light ($\lambda < 350$ nm) only. This result corresponded well with the UV–vis diffuse reflectance spectra. The hydrogen evolution over pure PbS was observed to be 0.34 mmol/g. It was observed that the PbS(25 wt.%)/$K_2Ti_4O_9$ showed the highest photo-catalytic activity among all catalysts and the amount of hydrogen evolved was 1.85 mmol/g. According to the aforementioned UV–vis diffuse reflection analysis, the deposition of PbS gave rise to a remarkable enhancement for visible light absorption.

The data in Fig. 10 further confirmed that the PbS concentration strongly influenced the efficiency of the prepared $PbS/K_2Ti_4O_9$ catalyst for photo-catalytic hydrogen production. The hydrogen evolution increased with increasing deposition of PbS, and a maximum activity (1.85 mmol/g) was exhibited at 25 wt.%. It should be noted that excessive deposition resulted in lower activities. It can be deduced that an optimum mixing ratio exists between PbS and $K_2Ti_4O_9$ for efficient hydrogen production. This was mainly because when loading amount of PbS was low, efficient areas on PbS irradiated by visible light was also less. So the amount of carrier excited by visible light was less and composite catalysts

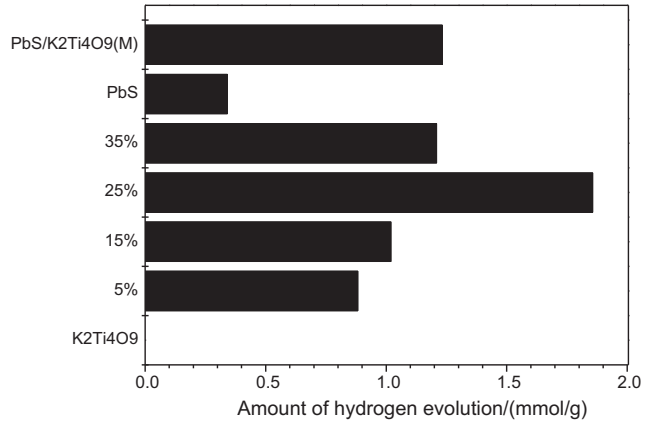

Fig. 10. Photo-catalytic hydrogen production activity of photo-catalysts under visible light.

exhibited poor photocatalytic performance. While loading amount of PbS is considerable large, the excessive deposition of PbS might have shaded the active sites for hydrogen generation on the surface of $K_2Ti_4O_9$. This would lead active sites for hydrogen production decrease and photocatalytic activity reduced.

The synthesis method used was also found to have a strong influence on the photo catalytic activity. As can be seen from Fig. 10, the catalyst with 25 wt.% PbS deposition exhibited the highest activity among the samples synthesized via precipitation, and the hydrogen evolved was 1.85 mmol/g. This was much higher than that of PbS(25 wt.%)/$K_2Ti_4O_9$(M), where only 1.23 mmol/g H_2 was produced. These results suggests that preparation method had a strong influence on the photocatalytic activity. According to SEM analysis, the prepared $PbS/K_2Ti_4O_9$ possessed uniform and nano-sized PbS particles. Smaller particle size could shorten the transfer time of electrons from the interior of PbS to the surface, thus decrease the recombination probilities of photo-induced electrons and holes [30]. While the pure PbS synthesized agglomerated together. When pure PbS was directly blended with $K_2Ti_4O_9$, PbS could not be well distributed on $K_2Ti_4O_9$, and thus the relatively low surface coverage of PbS may have resulted in the poor absorption of photons and generation of less photo-induced carriers. According to UV–vis diffuse reflectance analysis, in the visible region, the absorption spectra of composite catalyst synthesized by deposition–precipitation method was superior than that of the same loading amount catalyst synthesized by mechanical mixing, indicating that PbS in the composite catalysts synthesized by deposition–precipitation method showed better dispersity. Meanwhile, relatively higher dispersity of PbS lead to $PbS/K_2Ti_4O_9$ have a strong absorption for visible light, so catalyst synthesized by precipitation method generated more charge carriers in the visible region and showed better photo catalysis activity. Moreover, there may exist the Ti–O–Pb (refer to XPS analysis), promoting photo-induced carriers migration between semiconductors (refer to PL analysis), which may be another reason responded for the high activity.

3.3. Reaction mechanism

The photo-catalysis results showed the remarkable photo-catalytic activity of $PbS/K_2Ti_4O_9$ samples on hydrogen evolution under visible light irradiation. Based on literature [31] and our experimental results, we propose a mechanism for photo catalytic water-splitting hydrogen production on $PbS/K_2Ti_4O_9$ catalyst under visible light irradiation as shown in Fig. 11. Using two semiconductors in contact with different redox energy levels of their CB and VB, the efficiency of photo generated carriers separation and the interfacial charge transfer can be enhanced.

The band structure of the semiconductor plays an important role in the improvement of photo-catalytic activity. Using two semiconductors in contact with different redox energy levels of CB and VB can enhance the efficiency of photo generated carriers separation and the interfacial charge transfer. The band gap of PbS is only 0.41 eV, so PbS shows good absorption for visible light. Semiconductor $K_2Ti_4O_9$ has no ability to absorb visible light due to its band gap of 3.54 eV, and is only responsive to UV light.

Energy band couplings were formed when PbS was combined with TiO_2 [32] or PbSe [33], within which, hence, potential barrier electric field between two phases was set up and the efficiency of charge separation was improved, extending the lifetime of charge carrier. This energy level match is helpful for promoting photo catalysis activity. Here, we suppose that the similar energy band coupling was formed with large contact area at the surface of $K_2Ti_4O_9$, when PbS being loaded on $K_2Ti_4O_9$. Generally, the band edge positions between two semiconductors at an interface are the key points for the efficient inter-particle transfer of photo-induced charge carriers. The conduction band and valence band of

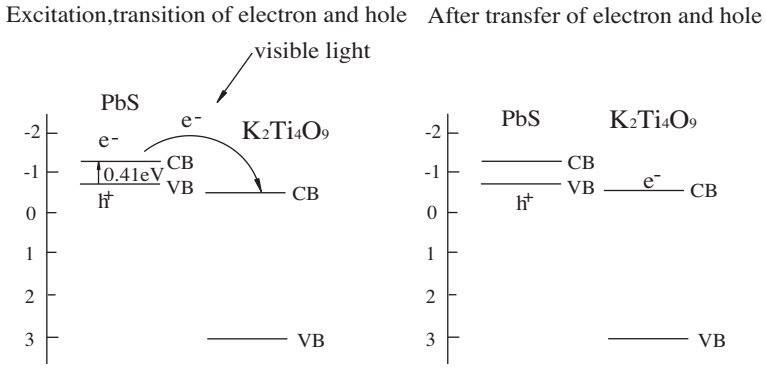

Fig. 11. Electron and hole transition of photo-catalysts under visible light.

PbS are −1.19 and −0.78 eV vs NHE, respectively [31]. As for $K_2Ti_4O_9$, the valence band position is +3.0 eV vs NHE and the conduction band position is −0.54 eV vs NHE. When irradiated under visible light, PbS in the composite photocatalyst absorbs photons and excites electron and hole pairs. The electric field at the PbS/$K_2Ti_4O_9$ interface pushes the photo-generated electrons toward the conduction band of $K_2Ti_4O_9$, and the electrons further migrate into the inner surface of the layered compounds of $K_2Ti_4O_9$ [29], while the photo-generated holes stay on the valence band of PbS. Therefore, the photo excited electrons can be effectively collected by $K_2Ti_4O_9$, and holes collected by PbS.

The photo-generated electrons in the conduction band could reduce H_2O to H_2, while the photo-generated holes in the valence band can oxidize S^{2-} and SO_3^{2-} to form S_2^{2-} and SO_4^{2-}, respectively. The production of S_2^{2-} ions, which act as an optical filter and compete with the reduction of protons, was efficiently suppressed by mixing with SO_3^{2-} ions. The presence of excess S^{2-} ions also act to stabilize the photo-catalyst surface because the formation of sulfur defects could be suppressed [34]. The photo-catalytic process can be described as follows:

$$Photocatalyst \xrightarrow{visible-light} h^+ + e^-$$

$$2e^- + 2H_2O \rightarrow H_2 + 2OH^-$$

$$2S^{2-} + 2h^+ \rightarrow S_2^{2-}$$

$$SO_3^{2-} + H_2O + 2h^+ \rightarrow SO_4^{2-} + 2H^+$$

$$S_2^{2-} + SO_3^{2-} \rightarrow S_2O_3^{2-} + S^{2-}$$

$$S^{2-} + SO_3^{2-} + 2h^+ \rightarrow S_2O_3^{2-}$$

4. Conclusions

Novel PbS-sensitized $K_2Ti_4O_9$ composite (PbS/$K_2Ti_4O_9$) photocatalysts were prepared through a precipitation method. The PbS/$K_2Ti_4O_9$ samples displayed strong light absorption in the visible light region and exhibited enhanced photo-catalytic performance for hydrogen evolution under visible light irradiation. The highest activity of 1.85 mmol/g was achieved using 25 wt.% PbS/$K_2Ti_4O_9$ prepared via precipitation method. The mechanism of separation of the photogenerated electrons and holes at the PbS/$K_2Ti_4O_9$ composite was discussed.

Acknowledgment

This work was supported by the National Natural Science Foundation of China (Grant Nos. 50972037 and 51172063).

References

[1] A. Fujishima, X. Zhang, D.A. Tryk, Int. J. Hydrogen Energy 32 (2007) 2664–2672.
[2] M. Matsuoka, M. Kitano, M. Takeuchi, et al., Catal. Today 122 (2007) 51–61.
[3] O. Eneat, Allen J. Bard, J. Phys. Chem. 90 (1986) 301–306.
[4] W. Cui, Y. Liu, Li Liu, J. Hu, Y. Liang, Appl. Catal. A: Gen. 417 (2012) 111–118.
[5] W. Cui, L. Liu, L. Feng, C. Xu, Z. Li, S. Lv, F. Qiu, Sci. China Ser. B: Chem. 149 (2) (2006) 162–168.
[6] F.E. Osterloh, Chem. Mater 20 (2008) 35–54.
[7] M.A. Bizeto, A.L. Shiguihara, V.R.L. Constantino, J. Mater. Chem. 19 (2009) 2512–2525.
[8] Y. Hosogi, H. Kato, A. Kudo, J. Phys. Chem. C 112 (2008) 17678–17682.
[9] M. Shibata, A. Kudo, A. Tanaka, et al., Chem. Lett. (1987) 1017–1018.
[10] J. Wang, H. Li, H. Li, et al., Solid State Sci. 11 (2009) 988–993.
[11] J. Wu, Y. Huang, T. Li, et al., Scripta Mater. 54 (2006) 1357–1362.
[12] R. Wang, D. Xu, J. Liu, et al., Chem. Eng. J. 168 (2011) 455–460.
[13] W. Shangguan, A. Yoshida, Sol. Energy Mater. Sol. Cells 69 (2001) 189–194.
[14] W. Cui, Y. Qi, L. Liu, D. Rana, J. Hu, Y. Liang, Prog. Nat. Sci. Mater. Int. 22 (2012) 120–125.
[15] K. Mogyorósi, I. Dékány, J.H. Fendler, Langmuir 19 (2003) 2938–2946.
[16] Y. Ji, L. Black, P.G. Weidler, et al., Langmuir 20 (2004) 9796–9806.
[17] F. Jiang, Z. Zheng, Z. Xu, et al., J. Hazard. Mater. 164 (2009) 1250–1256.
[18] Y. Tang, J. Nian, B. Yu, et al., Mater. Lett. 63 (2009) 1992–1994.
[19] J. Yang, Q. Liu, X. Sun, Mater. Lett. 61 (2007) 1855–1858.
[20] J. Choy, H. Lee, H. Jung, et al., J. Mater. Chem. 11 (2001) 2232–2234.
[21] N.K. Mudugamuwa, D.M.N.M. Dissanayake, A.A.D.T. Adikaari, S.R.P. Silva, Sol. Energy Mater. Sol. Cells 93 (2009) 549–551.
[22] S.Y. Jang, Y.M. Song, H.S. Kim, Y.J. Cho, Y.S. Seo, G.B. Jung, C.W. Lee, J. Park, M. Jung, J. Kim, B. Kim, J. Kim, Y. Kim, ACSNANO 4 (2010) 2391–2401.
[23] J.F. Moulder, W.F. Stickle, P.E. Sobol, K.D. Bomben, Perkin Elmer Corp. Eden Prairie, MN, 1992.
[24] J. Akhtar, M.A. Malik, P. O'Brien, K.G.U. Wijayantha, R. Dharmadasa, S.J.O. Hardman, D.M. Graham, B.F. Spencer, S.K. Stubbs, W.R. Flavell, D.J. Binks, F. Sirotti, J. Mater. Chem. 20 (2010) 2336–2344.
[25] L. Pauling, The Nature of the Chemical Bond, 3rd ed., Cornel University Press, Ithaca N.Y, New York, 1960. pp. 126.
[26] H. Chen, K. Young, Y.L. Kuo, Water Res. 41 (2007) 2067–2078.
[27] A. Kudo, T. Sakata, J. Phys. Chem. 99 (1995) 15963–15967.
[28] E. Thimsen, S. Biswas, S.L. Cynthia, P. Biswas, J. Phys. Chem. C 113 (2009) 2014–2021.
[29] K. Domen, Y. Ebina, T. Sekine, A. Tanaka, J. Kondo, C. Hirose, Catal. Today 16 (1993) 479.
[30] A.L. Stroyuk, A.I. Kryukov, S.Y. Kuchmii, V.D. Pokhodenko, Theoret. Exp. Chem. 41 (4) (2005) 207–228.
[31] R. Brahimi, Y. Bessekhouad, A. Bouguelia, M. Trari, J. Photochem. Photobiol. A: Chem. 194 (2008) 173–180.
[32] C. Ratanatawanate, Y. Tao, K.J. Balkus, J. Phys. Chem. C 113 (2009) 10755–10760.
[33] D. Cui, J.n. Xu, G. Paradee, S. Xu, Y. Wang, J. Exp. Nanosci. 2 (2007) 13–21.
[34] I. Tsuji, H. Kato, H. Kobayashi, A. Kudo, J. Am. Chem. Soc. 126 (2004) 13406–13413.